Synthesis of $Cu_yMn_zAl_{1-z}O_x$ mixed oxide as low-temperature NH_3-SCR catalyst with enhanced catalytic performance

Qinghua Yan[1], Sining Chen[1], Lei Qiu[1], Yanshan Gao[1], Dermot O'Hare[2], Qiang Wang[1,*]

[1]College of Environmental Science and Engineering, Beijing Forestry University, 35 Qinghua East Road, Haidian District, Beijing 100083, P. R. China

[2]Chemistry Research Laboratory, Department of Chemistry, University of Oxford, 12 Mansfield Road, Oxford, OX1 3TA, UK

*Corresponding author:

College of Environmental Science and Engineering, Beijing Forestry University, 35 Qinghua East Road, Haidian District, Beijing 100083, P. R. China

E-mail: qiang.wang.ox@gmail.com; qiangwang@bjfu.edu.cn

Tel: +86 13699130626

Abstract

A new type of low-temperature selective catalytic reduction (SCR) catalyst $Cu_yMn_zAl_{1-z}O_x$ derived from layered double hydroxides was designed. By tuning the ratio of Cu/Mn/Al, the optimal NH_3-SCR performance was achieved with the chemical composition of $Cu_2Mn_{0.5}Al_{0.5}O_x$. At 150 °C, a high NO_x conversion of 91.2% was achieved with $Cu_2Mn_{0.5}Al_{0.5}O_x$, which is much higher than that of all other control catalysts Cu_2AlO_x (71.1%), Cu-Mn/γ-Al_2O_3 (65.23%), and Mn/γ-Al_2O_3 (59.32%). Catalysts were characterized in detail using various physico-chemical techniques including XRD, BET, FTIR, TEM, H_2-TPR, NH_3-TPD, and XPS analyses, and the results revealed that the superior catalytic performance of $Cu_2Mn_{0.5}Al_{0.5}O_x$ catalyst can be attributed to its high specific surface area, high reducibility of MnO_2 and CuO species, abundance of surface acid sites, and well dispersion of MnO_2 and CuO species. $Cu_2Mn_{0.5}Al_{0.5}O_x$ also showed much higher resistance to 100 ppm SO_2 and 5% H_2O than the control catalysts. The poisoning mechanism and the regenerability of $Cu_2Mn_{0.5}Al_{0.5}O_x$ catalyst was also investigated. In all, compared with the control catalysts of Cu_2AlO_x, Cu-Mn/γ-Al_2O_3, and Mn/γ-Al_2O_3, the newly designed $Cu_2Mn_{0.5}Al_{0.5}O_x$ catalyst is not only more active at low temperatures (100–250 °C), but also relatively more robust in the presence SO_2 and H_2O.

Keywords: selective catalytic reduction; Mn-based catalyst; layered double hydroxides; sulfur dioxide; regenerability

1. Introduction

The emissions of nitrogen oxides (NO_x) from power plant and municipal solid waste (MSW) incineration plant are known to cause damages to human health and environmental safety. The removal of nitrogen oxides from the flue gas has become an important issue. As the most effective method for the abatement of NO_x emission from stationary resources, selective catalytic reduction (SCR) process has been put into widely commercial utilization during the past several decades.[1, 2]

The backbone of SCR technology is the development of SCR catalysts such as noble metals based,[3] supported metal oxides based,[4] zeolites based,[5] and many others.[6-8] Among them, vanadia-based catalyst is known to be the most effective and widely used commercial SCR catalyst due to its high activity and durability to SO_2. Because this catalyst exhibits good performance only in a narrow temperature window of 300–400 ^oC, the SCR unite should be applied before units for electrostatic precipitator and desulphurization in order to avoid reheating of the flue gas.[9] However, the flue gas from incinerators has high concentrations of particles and other contaminants which cause the deactivation of catalysts. Therefore, for this reason, there is a strong interest in the development of SCR catalysts at lower temperatures (< 300 ^oC). Low-temperature SCR catalysts would be placed downstream the desulfurizer and electrostatic precipitator, and the temperature at this point is 150−160 ^oC. Success in developing such catalysts would significantly improve the economics of SCR. Moreover, there is still residual SO_2 remaining after the desulfurizer. Thus, SO_2 resistance needs to be considered as well.

To date, a large number of catalysts consisted of various transition metal (V, Cr, Mn, Fe, Co, Ni and Cu) oxides on different commercial supports such as titania and alumina have been studied for low temperature SCR reactions. Among these catalysts,

Mn-based catalysts such as MnO_x/Al_2O_3,[10] MnO_x/NaY,[11] MnO_x/USY,[12] and MnO_x/TiO_2[13, 14] have attracted interest because of its high SCR activity at low temperature. The manganese oxides contain various types of labile oxygen, which is necessary to complete oxidation–reduction cycle.[15, 16] However, Mn-based SCR catalyst still suffers the deactivation by SO_2. In order to enhance the SCR activity and SO_2 resistance of Mn-based catalyst, several transition metals (such as Ni, Ce, Cu, Fe, Co, etc.) have been used to modify the Mn-based catalysts.[17-22] Recently, Cu-based catalyst have received much attention due to its capability of simultaneous removal of SO_2 and NO_x from flue gases. [23, 24] Therefore, In order to enhance the SCR activity and SO_2 resistance of Mn-based catalysts, copper transition metal be considered introducing to modify the Mn-based catalysts. In addition, there were some investigations on the synthesis of highly dispersed mixed metal oxides based catalysts via the careful calcination of a highly dispersed layered double hydroxides (LDHs) precursors.[25] Using this approach the dispersion of active metal species can be controlled at the atomic level.[26-29]

In the present work, we report a new low-temperature SCR catalyst $Cu_yMn_zAl_{1-z}O_x$ from CuMnAl-CO_3 LDH with enhanced SCR activity and SO_2 resistance. Synthesized catalyst were characterized using XRD, BET, SEM, TEM, FTIR, XPS, NH_3-TPD, and H_2-TPR in order to illustrate the influence of Cu modification and the advantages of using LDH precursor. The optimized catalyst with a composition of $Cu_2Mn_{0.5}Al_{0.5}O_x$ exhibited a NO_x conversion as high as 91.2% at 150 ^oC. It also showed higher SO_2 resistance than the control catalysts Cu_2AlO_x LDO, Cu-Mn/γ-Al_2O_3, and Mn/γ-Al_2O_3. The influence of H_2O on the catalytic activity of $Cu_2Mn_{0.5}Al_{0.5}O_x$ catalyst was also evaluated. We hope that this work could guide us to design highly efficient Mn-based SCR catalysts with excellent low-temperature activity and SO_2 resistance.

2. Experimental

2.1 Preparation of $Cu_yMn_zAl_{1-z}O_x$ (y = 1–4) and Cu_2AlO_x mixed oxide catalysts

For the synthesis $Cu_yMn_zAl_{1-z}$-CO_3 LDHs, a standard co-precipitation method was used. An aqueous solution containing nitrates of the metallic salts $Cu(NO_3)_2 \cdot 6H_2O$, $Al(NO_3)_3 \cdot 9H_2O$, and 50% $Mn(NO_3)_2$ with different M^{2+}/M^{3+} ratios (1, 2, 3, and 4) and different Mn^{3+}/Al^{3+} ratios (1:1, 1:3, and 3:1) was added dropwise into a vigorously stirred Na_2CO_3 solution. During the synthesis, the temperature of mixture solution was maintained at 60 °C and the pH of the mixture solution was kept constant at 10 by addition of NaOH solution (4 M). The resulting slurry was stirred continuously for about 12 h at 60 °C. After aging, the precipitate was filtered and washed several times with deionized water until pH=7, then stirred in acetone for 2 h and washed with acetone. Finally, $Cu_yMn_zAl_{1-z}$-CO_3 LDHs were obtained by drying at 60 °C for 24 h in an oven. After being calcined at 400 °C for 5 h in air, various $Cu_yMn_zAl_{1-z}O_x$ mixed oxides were obtained, which were denoted as $Cu_1Mn_{0.5}Al_{0.5}O_x$, $Cu_2Mn_{0.5}Al_{0.5}O_x$, $Cu_3Mn_{0.5}Al_{0.5}O_x$, $Cu_4Mn_{0.5}Al_{0.5}O_x$, $Cu_2Mn_{0.25}Al_{0.75}O_x$, and $Cu_2Mn_{0.75}Al_{0.25}O_x$. Cu-Al-$CO_3$ LDH and the corresponding LDO Cu_2AlO_x can be obtained similarly.

2.2 Preparation of Mn/γ-Al_2O_3 and Cu-Mn/γ-Al_2O_3 catalysts

For comparison, the Mn/γ-Al_2O_3 and Cu-Mn/γ-Al_2O_3 catalysts were prepared by a conventional incipient wetness impregnation method. For Mn/γ-Al_2O_3, 2 wt% Mn was loaded on the γ-Al_2O_3 carrier. 2.5 g γ-Al_2O_3 solid was impregnated with 10 mL aqueous solution containing 0.2 mL $Mn(NO_3)_2$. For Cu-Mn/γ-Al_2O_3, the molar ratio of Cu/Mn was fixed at 4:1. 2.5 g γ-Al_2O_3 solid was impregnated with 10 mL aqueous solution containing 0.2 mL $Mn(NO_3)_2$ and 0.88 g $Cu(NO_3)_2 \cdot 6H_2O$. Subsequently, the impregnated samples were first dried at 60 °C for 24 h in an oven, followed by

calcination at 400 ºC in air for 5 h. The loadings of Cu and Mn metals are based on γ-Al_2O_3 support.

2.3 Characterization of catalysts

X-ray powder diffraction (XRD) patterns of the as-synthesized and calcined samples were measured using a Shimadzu XRD-7000 instrument in reflection mode using Cu Kα radiation. The X-ray tube was operated at 40 kV and 40 mA. The accelerating voltage was set at 40 kV with 30 mA current (λ = 1.542 Å). Diffraction patterns were recorded within the range of 2θ = 5–75º with a scanning rate of 5º/min and a step size of 0.02º. The morphology of samples was characterized using field emission scanning electron microscope (FE-SEM, SU-8010, Hitachi). Fourier transform infrared spectrometer (FT-IR) experiments were performed on a FTS 3000 MX FT-IR (Bruker Vertex 70) spectrophotometer in the range of 4000 to 400 cm^{-1} using the diamond ATR technique. One hundred scans were taken with a resolution of 4 cm^{-1} and all spectra were background corrected. Specific surface areas (SSA) of samples were measured with a physisorption analyser (SSA–7000, Builder). Before each measurement, about 0.1 g catalyst sample was degassed in a N_2/He mixture at 220 ºC for 4 h. X-ray photoelectron spectroscopy (XPS) analysis was performed on a Thermo Scientific Escalab 250Xi instrument, using monochromatic Al kα radiation (hν=1486.6 eV) operating at an accelerating power of 15 kW. Before the measurement, the sample was outgassed at room temperature in a UHV chamber (<5 $\times 10^{-7}$ Pa). The sample charging effects were compensated by calibrating all binding energies (BE) with the adventitious C 1s peak at 284.6 eV. This reference gave BE values with an accuracy at ±0.1 eV.

Temperature-programmed desorption of ammonia (NH_3-TPD) experiments were performed to determine the surface acidity of catalysts, which were carried out on a

fixed-bed continuous flow microreactor equipped with a quadrupole mass spectrometer (QGA, Hidden, UK). Prior to each measurement, about 0.15 g sample was first pretreated in highly purified Ar flow (40 mL/min) at 400 ^{o}C for 30 min. Then the reactor was cooled to 80 ^{o}C and the sample was kept under 1% NH_3/Ar flow (40 ml/min) for about 2 h. The catalyst was then purged in Ar to remove gaseous and weakly adsorbed (physisorbed) NH_3, until achieving a constant level of a signal. Then desorption was started from 80 to 650 ^{o}C with a linear heating rate of 2 ^{o}C/min in a flow of Ar (40 ml/min).

Temperature-programmed reduction (H_2-TPR) experiments were carried out on a multifunction chemisorption analyzer (PCA-1200, Builder) with a quartz U-tube reactor, detected by a thermal conductivity detector (TCD). For each test, about 0.15 g sample was utilized. Before switching to the H_2-Ar stream, the sample was pretreated in Ar stream (40 mL/min) at 200 ^{o}C for 30 min, and then cooled to 50 ^{o}C. The sample was heated from 50 to 650 ^{o}C with a ramping rate of 10 ^{o}C/min under 5% H_2/Ar mixture flow (30 mL/min).

2.4 Catalytic activity tests

The NH_3-SCR catalytic activity tests of synthesized catalysts were carried out at atmospheric pressure in a fixed-bed stainless steel reactor with an internal diameter of 10 mm. The stainless steel reactor was installed in a vertical split-tube furnace. For each test, 0.15 g catalyst was charged. After the reactor was heated up to the desired reaction temperature, the inlet gas containing 500 ppm NO_x, 500 ppm NH_3, 5% O_2, and balance Ar was fed to the reactor with a flow rate of 200 mL/min. Afterwards, to determine the impact of SO_2 on the activity, the catalysts were studied by introducing 100 ppm SO_2 to the inlet gas (500 ppm NO_x, 500 ppm NH_3, 5% O_2, 100 ppm SO_2, balance Ar). All

the gas flows were controlled independently by mass flow controllers (Brooks Instruments). The NO_x concentrations in the inlet and outlet gases were continuously analyzed using an on-line NO_x analyzer (Thermo Scientific 42i-HL, USA). The NO_x conversion at steady state was calculated using the follow equation (1). The deactivated catalysts were regenerated by heating the samples in air at a heating rate of 5 ºC/min to 400 ºC and held at this temperature 1 h purging with air.

$$NOx \text{ conversion} = \left(1 - \frac{NOx(out)}{NOx(in)}\right) \times 100\% \quad (1)$$

3. Results and discussion

3.1 Characterization of $Cu_yMn_zAl_{1-z}$-CO_3 LDHs

Fig. 1(a) shows the XRD patterns of synthesized $Cu_yMn_zAl_{1-z}$-CO_3 LDHs precursors with different Cu/(Mn+Al) molar ratios of 1, 2, 3, or 4 and Mn/Al molar ratio of 1. All samples presented the characteristic diffraction peaks of layered double hydroxide structure without any impurity phases, suggesting the complete incorporation of transition metals Mn and Cu into the crystalline structure. Sharp and intense Bragg reflections at 2θ = 11.72º, 23.53º, 34.59º, 39.44º, and 46.86º, can be indexed to the (003), (006), (012), (015), and (018) planes of $Cu_yMn_zAl_{1-z}$-CO_3 LDHs unit cell, respectively. Comparing to the typical Mg-Al-CO_3 LDH (JCPDS: 41-1428), the diffraction peaks slightly shifted to higher angles. This phenomenon can be explained by the distortion of the copper sites, which is caused by the Jahn–Teller effect of Cu^{2+} (d^9) as reported by previous work.[30]

In addition, the $Cu_yMn_zAl_{1-z}$-CO_3 LDHs derived mixed oxides $Cu_yMn_zAl_{1-z}O_x$ were also analyzed. Fig. 1(b) shows that the layered structure of all LDHs transformed into mixed oxides after being calcined at 400 ºC. In all samples, the diffraction peaks

can be ascribed to the formation of crystallized CuO (JCPDS: No. 45-0937). No manganese oxide related crystalline phases was found, which indicates that Mn was finely dispersed within the mixed oxides.

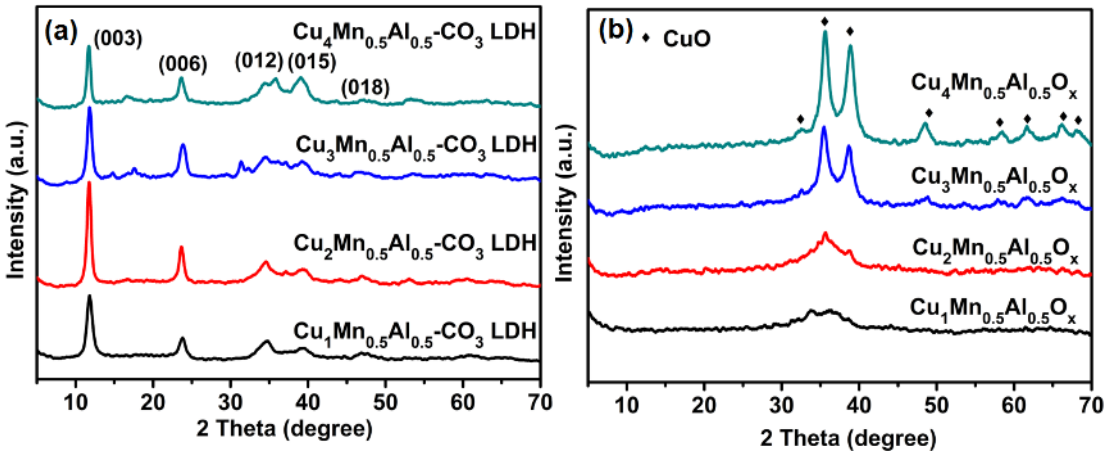

Fig. 1. XRD patterns of (a) $Cu_yMn_zAl_{1-z}$-CO_3 LDHs synthesized with different Cu/Al ratios, and (b) $Cu_yMn_zAl_{1-z}O_x$ calcined at 400 °C.

The physical properties of LDHs and the corresponding LDOs were evaluated by BET measurements, as shown in Table 1. As it can be seen, the SSA of $Cu_yMn_zAl_{1-z}$-CO_3 LDHs became higher with the increase in Cu/(Mn+Al) molar ratio, from 115.60 to 153.48–168.23 m^2/g. After calcination, the SSA of obtained mixed oxides were slightly decreased to the range of 96–136 m^2/g. Among all mixed oxides, $Cu_2Mn_{0.5}Al_{0.5}O_x$ showed the highest SSA, which is favorable for improving the SCR activity at certain extent. It is well known that higher SSA could provide more available active sites on the catalyst surface for reactants to participate reactions.[31, 32] The morphology of synthesized $Cu_yMn_zAl_{1-z}$-CO_3 LDHs were studied using FE-SEM and TEM analyses. Fig. 2 revealed that the $Cu_2Mn_{0.5}Al_{0.5}$-CO_3 LDH possesses "flower-like" hierarchical morphology with typical well-defined nanoplatelets. Similar morphology has been reported by Gennequin et al. for Mg−Al LDH.[33]

Table 1. Specific surface area, pore size, and pore volume of $Cu_yMn_zAl_{1-z}$-CO_3 LDHs and the corresponding $Cu_yMn_zAl_{1-z}O_x$ LDOs.

Samples	BET SSA (m^2/g)	BJH Pore size (Å)	BJH pore volume (cm^3/g)
$Cu_1Mn_{0.5}Al_{0.5}CO_3$ LDH	115.60	142.4	0.823142
$Cu_2Mn_{0.5}Al_{0.5}CO_3$ LDH	168.23	124.2	1.044717
$Cu_3Mn_{0.5}Al_{0.5}CO_3$ LDH	153.48	112.6	0.863760
$Cu_4Mn_{0.5}Al_{0.5}CO_3$ LDH	157.94	122.0	0.963069
$Cu_1Mn_{0.5}Al_{0.5}O_x$ LDO	133.26	114.1	0.760285
$Cu_2Mn_{0.5}Al_{0.5}O_x$ LDO	136.45	150.9	1.029414
$Cu_3Mn_{0.5}Al_{0.5}O_x$ LDO	110.40	123.9	0.684070
$Cu_4Mn_{0.5}Al_{0.5}O_x$ LDO	96.20	116.2	0.558993

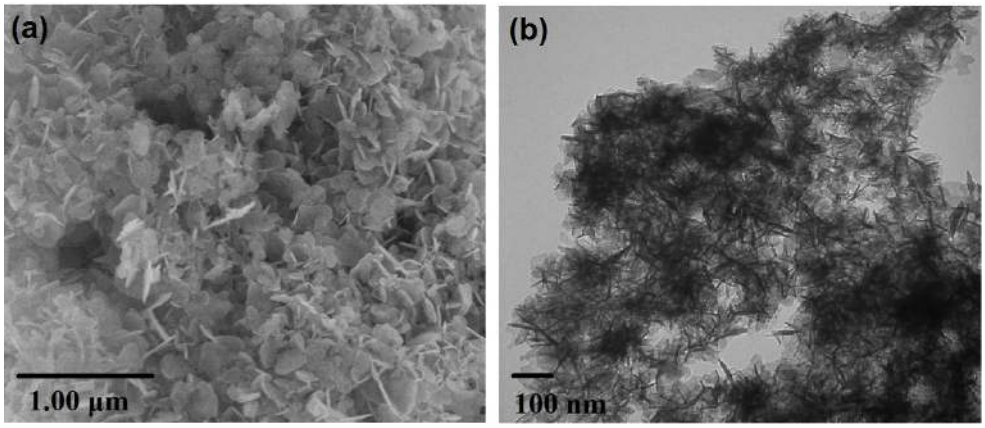

Fig. 2. (a) SEM and (b) TEM images of $Cu_2Mn_{0.5}Al_{0.5}$-CO_3 LDH.

Fig. 3 shows the FT-IR spectra of $Cu_yMn_zAl_{1-z}$-CO_3 LDHs and the corresponding LDOs. For fresh LDHs, similar FT-IR spectra to Mg−Al hydrotalcite were observed.[33] A broad absorption band centered at 3357 cm^{-1} is attributed to the stretching vibrations of –OH groups in the brucite-like layers, the lattice water and the interlayer water molecules. The vibration of angular deformation of H_2O molecules is observed at 1557 cm^{-1}. The absorption band at 1364 cm^{-1} in the spectra can be related to the vibrations of carbonate ions. Finally, the absorption bands around 838 and 570 cm^{-1} are attributed to the vibrations of the M–O (M–OH, M–O–M or O–M–O). Both XRD and FTIR data

confirmed the successful synthesis of $Cu_yMn_zAl_{1-z}$-CO_3 LDHs with different Cu/(Mn+Al) molar ratios.

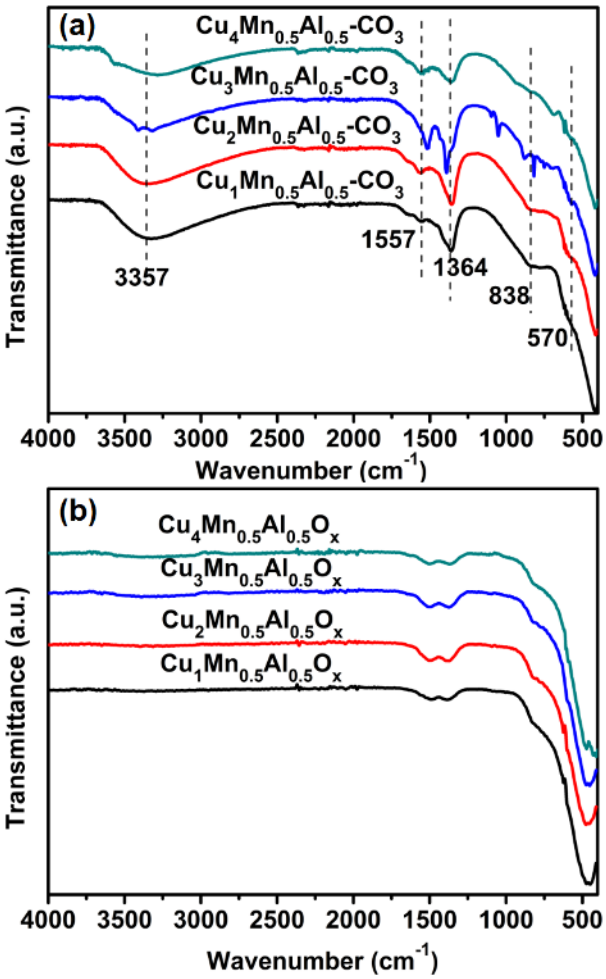

Fig. 3. FTIR spectra of (a) $Cu_yMn_zAl_{1-z}$-CO_3 LDHs with different Cu/(Mn+Al) ratios, and (b) $Cu_yMn_{0.5}Al_{0.5}O_x$ LDOs with different Cu/(Mn+Al) ratios obtained by calcining at 400 °C.

3.2 SCR activity of $Cu_yMn_zAl_{1-z}O_x$ mixed oxide catalysts

For the Mn-based SCR catalysts, it is apparent that the ratios of Cu/(Mn+Al) and Mn/Al will have a significant effect on the activity. Therefore, a series of $Cu_yMn_zAl_{1-z}O_x$ mixed oxides was studied for the SCR of NO_x. Fig. 4 shows the influences of Cu/(Mn+Al) ratio (1, 2, 3, and 4) and Mn^{3+}/Al^{3+} ratio (1:3, 1:1, and 3:1) on the activity of $Cu_yMn_zAl_{1-z}O_x$ mixed oxide catalysts in the reaction temperature range of 100–250 °C. Initially, we

optimized the M^{2+}/M^{3+} molar ratio of $CuMn_{0.5}Al_{0.5}O_x$ by changing the Cu/(Mn+Al) to be 1, 2, 3, and 4. The NO_x conversion at 150 °C first increased with the increase in Cu/(Mn+Al) ratio from 1 to 2, and then started to decrease when the Cu/(Mn+Al) ratio from 3 to 4. Under all same testing conditions, the NO_x conversion of $Cu_1Mn_{0.5}Al_{0.5}O_x$, $Cu_2Mn_{0.5}Al_{0.5}O_x$, $Cu_3Mn_{0.5}Al_{0.5}O_x$, and $Cu_4Mn_{0.5}Al_{0.5}O_x$ catalyst at 150 °C were 74.3%, 91.2%, 87.5%, and 76.9%, respectively. This data clearly indicated that the Cu/(Mn+Al) molar ratio has a strong influence on the SCR activity of catalysts, and the composition of $Cu_2Mn_{0.5}Al_{0.5}O_x$ exhibited the highest NO_x conversion of 91.2% at 150 °C (Fig. 4(a)).

After revealing the best M^{2+}/M^{3+} ratio, the impact of Mn^{3+}/Al^{3+} molar ratio (1:3, 1:1, and 3:1) was also studied, as shown in Fig. 4(b). At all temperatures ranging form 100 to 250 °C, the NO_x conversions all increased with the increase of Mn^{3+}/Al^{3+} molar ratio from 1:3 to 1:1. However, further increasing the Mn^{3+}/Al^{3+} molar ratio from 1:1 to 3:1 resulted in a decline in NO_x conversion. For instance, at 100, 150, 200, and 250 °C, the NO_x conversions were decreased from 51.6%, 91.2%, 83.6%, and 70.4% to 35.2%, 85.7%, 82.4%, and 67%, respectively. Previous researches have also demonstrated that there is always an optimal loading for the active component. When the loading of the active component was increased beyond a certain value, sintering would take place on the surface of catalysts and result in the formation of crystallization, thereby lowering the activity.[34, 35] In summary, the $Cu_2Mn_{0.5}Al_{0.5}O_x$ catalyst showed the best SCR catalytic performance with Cu/(Mn+Al) molar ratio being 2:1, and the Mn^{3+}/Al^{3+} molar ratio being 1:1, with a NO_x conversion of 91.2% at 150 °C.

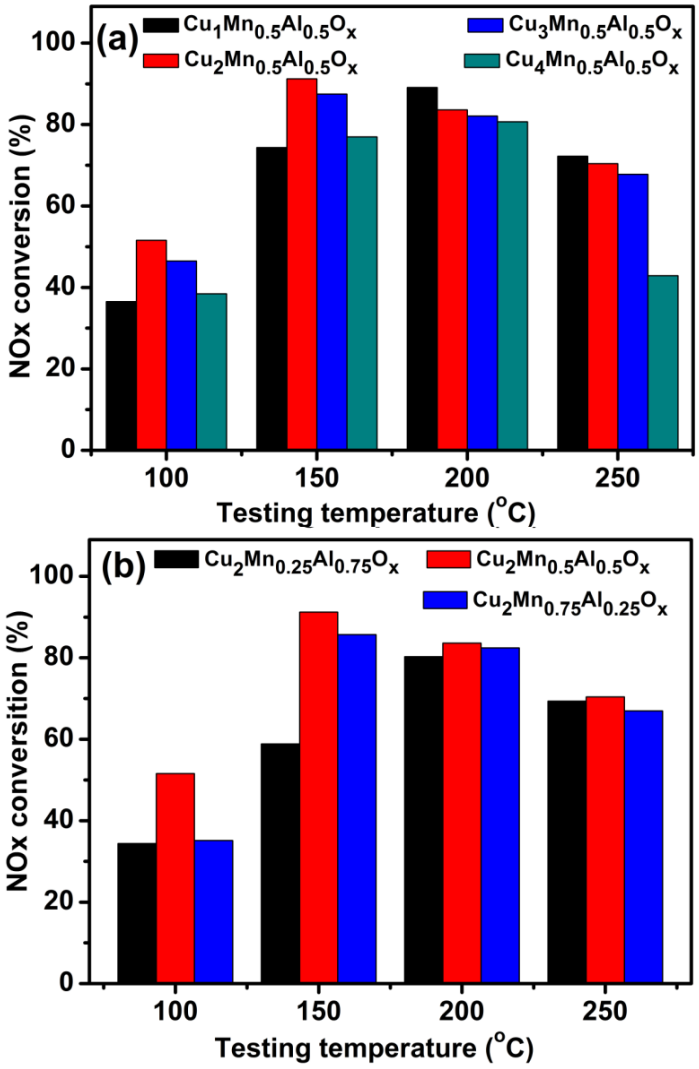

Fig. 4. The influence of (a) Cu/(Mn+Al) ratio (1, 2, 3, and 4), and (b) Mn^{3+}/Al^{3+} ratio (1:3, 1:1, and 3:1) on the activity of $Cu_yMn_zAl_{1-z}O_x$ mixed oxide catalysts. Calcination temperature = 400 °C, and operating temperature =100, 150, 200, and 250 °C. Reaction conditions: $[NO_x] = [NH_3]$ = 500 ppm, $[O_2]$ = 5%, balance Ar, total flow rate = 200 mL/min, catalyst 0.15 g.

3.3 Comparison of $Cu_2Mn_{0.5}Al_{0.5}O_x$, Cu_2AlO_x, Cu-Mn/γ-Al_2O_3, and Mn/γ-Al_2O_3 catalysts

Previously, there are a few reports on conventional supported Mn/Al_2O_3 as NH_3-SCR catalyst. For instance, Singoredjo et al.[10] and Kijlstra et al.[36] studied the catalytic

activity and SO_2 resistance of MnO_x/Al_2O_3 catalysts and found that they are very sensitive to SO_2. In addition, Kang et al.[20] investigated Cu-Mn mixed oxides catalyst, with which the deactivation phenomenon due to the presence of water vapor and SO_2 was also observed. In the following section, a comparative study on $Cu_2Mn_{0.5}Al_{0.5}O_x$, Cu_2AlO_x, Cu-Mn/γ-Al_2O_3, and Mn/γ-Al_2O_3 was performed. Fig. 5(a) shows the NO_x conversions of these four catalysts as a function of temperature for NH_3-SCR. For $Cu_2Mn_{0.5}Al_{0.5}O_x$ and Cu_2AlO_x samples, both of them exhibited better NO_x conversion compared with the supported catalysts of Mn/γ-Al_2O_3 and Cu-Mn/γ-Al_2O_3 at 100–250 ^oC. For $Cu_2Mn_{0.5}Al_{0.5}O_x$, the highest NO_x conversion was achieved at 200 ^oC, which was 91.2%. While the maximal NO_x conversions for Cu_2AlO_x, Cu-Mn/γ-Al_2O_3, and Mn/γ-Al_2O_3 catalysts were achieved at 200 ^oC, which are only 84.2%, 82.6%, and 67.2%, respectively. It is apparent that the $Cu_2Mn_{0.5}Al_{0.5}O_x$ catalyst possesses much better SCR performance than the other three catalysts, particularly in the temperature range of 150–200 ^oC. In addition, the optimal operating temperature of $Cu_2Mn_{0.5}Al_{0.5}O_x$ (150 ^oC) was also lower than that of other samples (200 ^oC). In all, it can be concluded that our newly designed catalyst $Cu_2Mn_{0.5}Al_{0.5}O_x$ possesses much better low-temperature SCR performance than other catalysts including Cu_2AlO_x, Cu-Mn/γ-Al_2O_3, and Mn/γ-Al_2O_3 catalysts.

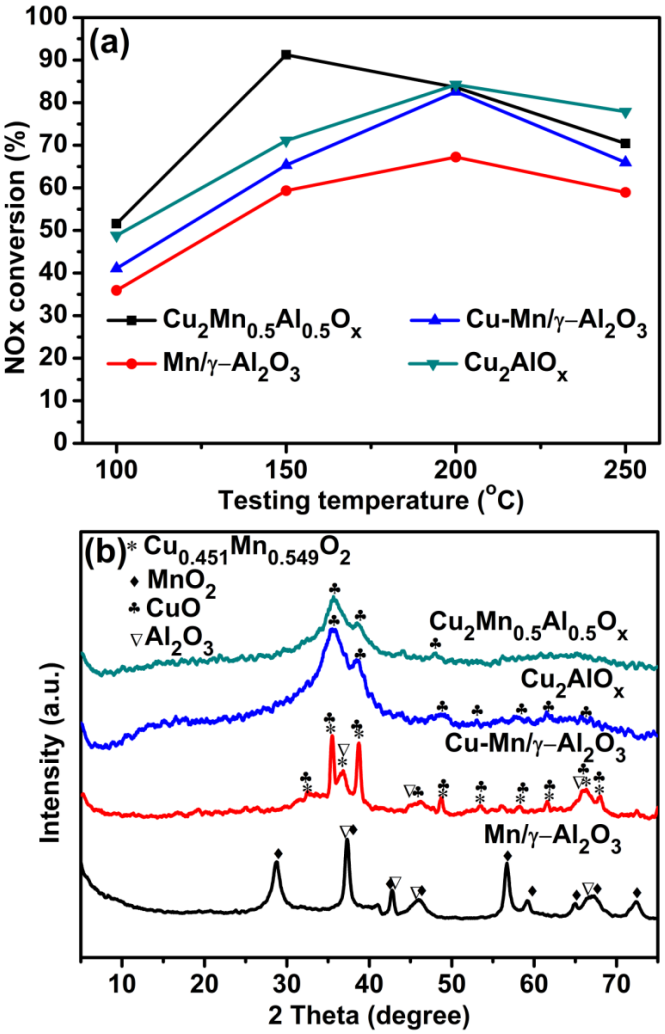

Fig. 5. (a) The NO_x conversion over $Cu_2Mn_{0.5}Al_{0.5}O_x$, Cu_2AlO_x, Cu-Mn/γ-Al_2O_3, and Mn/γ-Al_2O_3 catalysts as a function of temperature. (b) The XRD patterns of $Cu_2Mn_{0.5}Al_{0.5}O_x$, Cu_2AlO_x, Cu-Mn/γ-Al_2O_3, and Mn/γ-Al_2O_3 calcined at 400 °C. Operating temperature =100, 150, 200, and 250 °C. Reaction conditions: [NO_x] = [NH_3] = 500 ppm, [O_2] = 5%, balance Ar, total flow rate = 200 mL/min, catalyst 0.15 g.

In order to understand why the $Cu_2Mn_{0.5}Al_{0.5}O_x$ catalyst has better activity at low temperature than other catalysts, the XRD patterns of these catalysts were examined after being calcined at 400 °C, as shown in Fig 5(b). For Mn/γ-Al_2O_3, crystallized MnO_2 (JCPDS: No. 24-0735) and Al_2O_3 (JCPDS: No. 04-0880) were observed. While after introducing Cu, a mixture of oxides and spinel were detected for Cu-Mn/γ-Al_2O_3,

including CuO (JCPDS: No. 45-0937), Al_2O_3 (JCPDS: No. 04-0880) and $Cu_{0.451}Mn_{0.549}O_2$ (JCPDS: No. 41-0184) spinel phases. For $Cu_2Mn_{0.5}Al_{0.5}O_x$ and Cu_2AlO_x samples, only CuO phase was observed. No crystalline phase ascribed to manganese oxide can be found. It suggests that manganese oxide is finely dispersed as a non-crystalline phase or the particle size is smaller than the detection limit of XRD analysis. Moreover, aluminum oxide was not observed neither because it was in an amorphous state at this calcination temperature.[37] This may be ascribed to that the transition metal Cu has positive effect on the activity of catalysts and could reduce the crystallinity of manganese oxide and weaken the sintering in catalysts, which is in accordance with previous study. [38, 39]

The chemical composition and the oxidation state of manganese and copper in different catalysts were examined using XPS analyses. Fig. 6 shows the XPS spectra of Mn 2p, Cu 2p and O 1s of $Cu_2Mn_{0.5}Al_{0.5}O_x$, Cu_2AlO_x, Cu-Mn/γ-Al_2O_3, and Mn/γ-Al_2O_3 catalysts. The surface components of these samples were summarized in Table 2. The Mn 2p XPS profile indicated that MnO_x existed in the form of a mixed-valence manganese system on catalysts surface. Two main peaks corresponding to Mn 2p1/2 and Mn 2p3/2 were observed at around 632−658 eV for all samples. By performing peak-fitting deconvolutions, the Mn 2p3/2 of mixed-valence manganese system can be divided into two characteristic peaks, which can be attributed to Mn^{4+} (643.2 ± 0.2 eV) and Mn^{3+} (642.0 ± 0.2 eV), respectively.[40] The SCR of NO_x over the pure manganese oxides at the low temperature was investigated by Kapteijn et al.[41] They found that the De-NO_x efficiency decreased in the order of MnO_2 > Mn_5O_8 > Mn_2O_3 > Mn_3O_4. The relative concentrations of Mn^{4+} in this research follows the order of $Cu_2Mn_{0.5}Al_{0.5}O_x$ > Cu-Mn/γ-Al_2O_3 > Mn/γ-Al_2O_3. Previous studies have demonstrated that the higher oxidation state of manganese species (Mn^{4+}) was preferable for the redox properties of

manganese-based catalysts.[42, 43] Thus, the high concentration of Mn^{4+} in $Cu_2Mn_{0.5}Al_{0.5}O_x$ catalyst is favorable for its excellent low-temperature SCR activity.

Table 2. The surface components of $Cu_2Mn_{0.5}Al_{0.5}O_x$, Cu_2AlO_x, Cu-Mn/γ-Al_2O_3, and Mn/γ-Al_2O_3 catalysts obtained by XPS analyses.

Catalysts	Mn (at.%)	Cu (at.%)	O (at.%)	Mn^{4+} (%)	Cu^{2+} (%)	O_β (%)
$Cu_2Mn_{0.5}Al_{0.5}O_x$	9.1	13.15	32.74	67.7	93.5	65.3
Cu_2AlO_x	-	13.94	32.44	-	91.3	61.7
Cu-Mn/γ-Al_2O_3	1.63	1.8	56.8	66.8	86.3	56.9
Mn/γ-Al_2O_3	0.88	-	57.74	40.2	-	37.3

Fig. 6(b) presents the Cu 2p XPS spectra of $Cu_2Mn_{0.5}Al_{0.5}O_x$, Cu_2AlO_x and Cu-Mn/γ-Al_2O_3 catalysts. The satellite peaks at 938.0–945.0 eV and 960.0–965.0 eV, and the intense and broad photoelectron peaks at about 934 eV (Cu 2p3/2) and 955.0 eV (Cu 2p1/2) were observed for all the catalysts. The relative intensity of Cu^{2+} of $Cu_2Mn_{0.5}Al_{0.5}O_x$ (93.5%) is higher than that of Cu_2AlO_x (91.3%) and Cu-Mn/γ-Al_2O_3 (86.3%), which are favorable for the high NO_x conversion activity.

Fig. 6(c) shows the O 1s XPS spectra of $Cu_2Mn_{0.5}Al_{0.5}O_x$, Cu_2AlO_x, Cu-Mn/γ-Al_2O_3, and Mn/γ-Al_2O_3 catalysts. The O 1s spectra of all catalysts can be fitted into two peaks. The peak at lower binding energy (528.7–530.9 eV) corresponds to lattice oxygen (O_α), whereas the one at higher binding energy (531.4–532.5 eV) is related to the surface adsorbed oxygen (O_β).[44] It is worth to notice that the relative concentration ratio of O_β increased and reached the maximum value with $Cu_2Mn_{0.5}Al_{0.5}O_x$ catalyst, as shown in Table. 2. This implies that the synthesis of $Cu_2Mn_{0.5}Al_{0.5}O_x$ mixed oxide from LDH can resulted in more surface oxygen vacancies. It has been reported that the surface adsorbed oxygen (O_β) plays a key role in the SCR reaction due to its higher mobility.[45, 46] As reported by Liu et al. [47], the O_β can promote the oxidation of NO into

NO_2, and consequently facilitate the "fast SCR" reaction. For the Mn/γ-Al_2O_3 and Cu-Mn/γ-Al_2O_3 catalysts, their O_β amounts are notably lower than that of $Cu_2Mn_{0.5}Al_{0.5}O_x$ and Cu_2AlO_x samples. Based on the XPS analysis, it can be concluded that the high concentrations of Mn^{4+}, Cu^{2+} and O_β should also be partly responsible for the good NO_x conversion of $Cu_2Mn_{0.5}Al_{0.5}O_x$ catalyst.

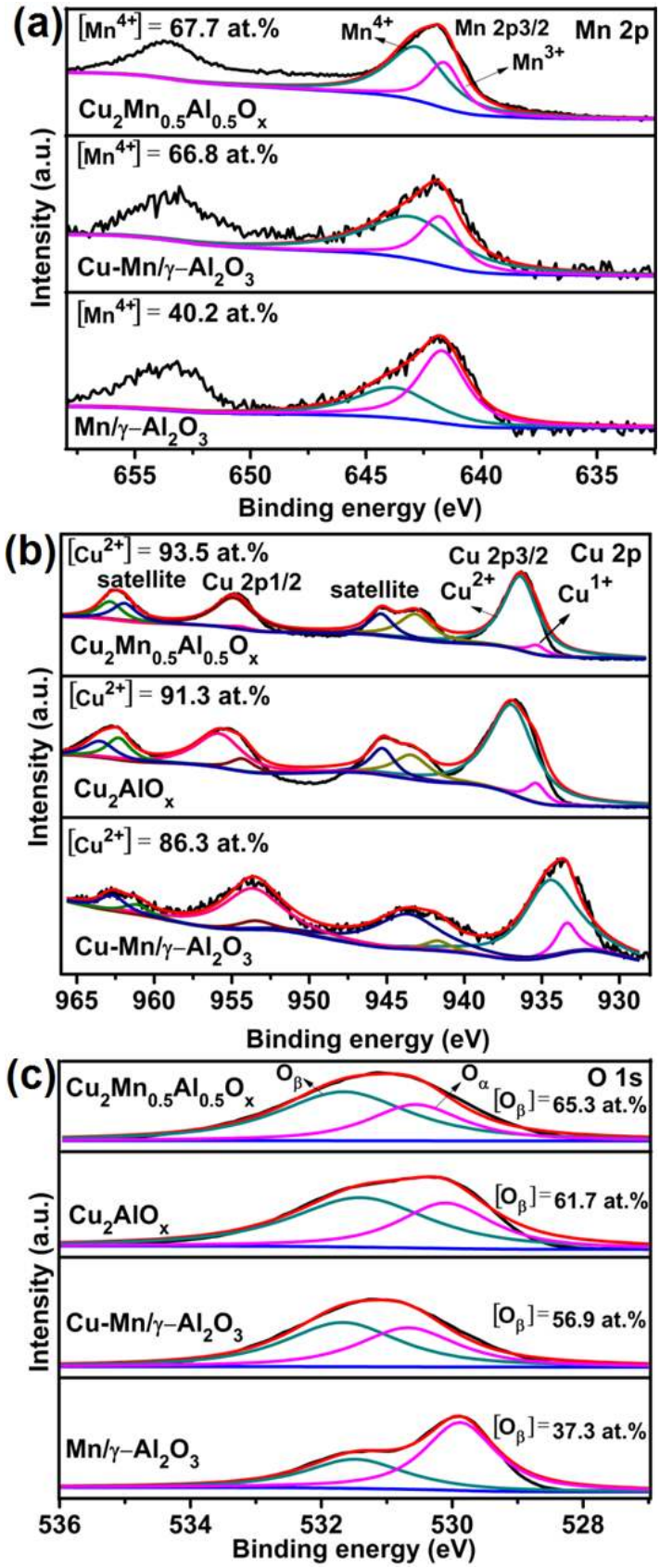

Fig. 6. XPS results of (a) Mn 2p, (b) Cu 2p, and (c) O 1s over $Cu_2Mn_{0.5}Al_{0.5}O_x$, Cu_2AlO_x, Cu-Mn/γ-Al_2O_3, and Mn/γ-Al_2O_3 catalysts.

The amount and strength of surface acidity of catalysts were probed by NH_3-TPD analysis. As shown in Fig. 7(a), NH_3 desorption is observed over a wide temperature range, due to the variability of adsorbed NH_3 species with different thermal stabilities. Desorption peaks of all samples located at about 150 °C. The amounts of desorbed NH_3 (surface acidity) over $Cu_2Mn_{0.5}Al_{0.5}O_x$, Cu_2AlO_x, Cu-Mn/γ-Al_2O_3, and Mn/γ-Al_2O_3 were compared by integrating the NH_3-TPD curves, and the area ratio among is approximately 2.58:1.24:1.16:1. This suggests that surface acidity of $Cu_2Mn_{0.5}Al_{0.5}O_x$ and Cu_2AlO_x is much higher than that of Cu-Mn/γ-Al_2O_3 and Mn/γ-Al_2O_3. The reaction mechanism of NH_3-SCR in the presence of excess oxygen has been investigated extensively and the surface acidity is considered to be closely related to the catalytic activity.[48]

The redox behaviors of catalysts were studied using H_2-TPR analysis, as shown in Fig. 7(b). Two reduction peaks for Mn/γ-Al_2O_3 were observed, which can be ascribed to the reduction of MnO_x species. In addition, the low-temperature reduction peak area of Cu-Mn/γ-Al_2O_3 and $Cu_2Mn_{0.5}Al_{0.5}O_x$ is significantly larger than that of Mn/γ-Al_2O_3. The enhancement maybe due to the synergistic effect between the copper and manganese oxide, which can create oxygen defects, and structural distortion. Thus, the synthesized $Cu_2Mn_{0.5}Al_{0.5}O_x$ mixed oxide from LDH possesses higher reducibility of MnO_x, implying the mobility of surface oxygen was enhanced and beneficial for the SCR reaction.[49, 50]

Compared with Mn/γ-Al_2O_3, the stepwise reduction peak of MnO_x for $Cu_2Mn_{0.5}Al_{0.5}O_x$ is broadened greatly due to the good dispersion of Mn species and its interaction with Cu. The broad reduction peak (150-500 °C) of $Cu_2Mn_{0.5}Al_{0.5}O_x$ catalyst could be assigned to the stepwise reduction of MnO_x, i.e., $MnO_2 \rightarrow Mn_2O_3 \rightarrow Mn_3O_4$

→ MnO, overlapped with the reduction of surface Cu^{2+}.[20] Moreover, the reduction peak area of $Cu_2Mn_{0.5}Al_{0.5}O_x$ is also larger than that of Cu_2AlO_x.

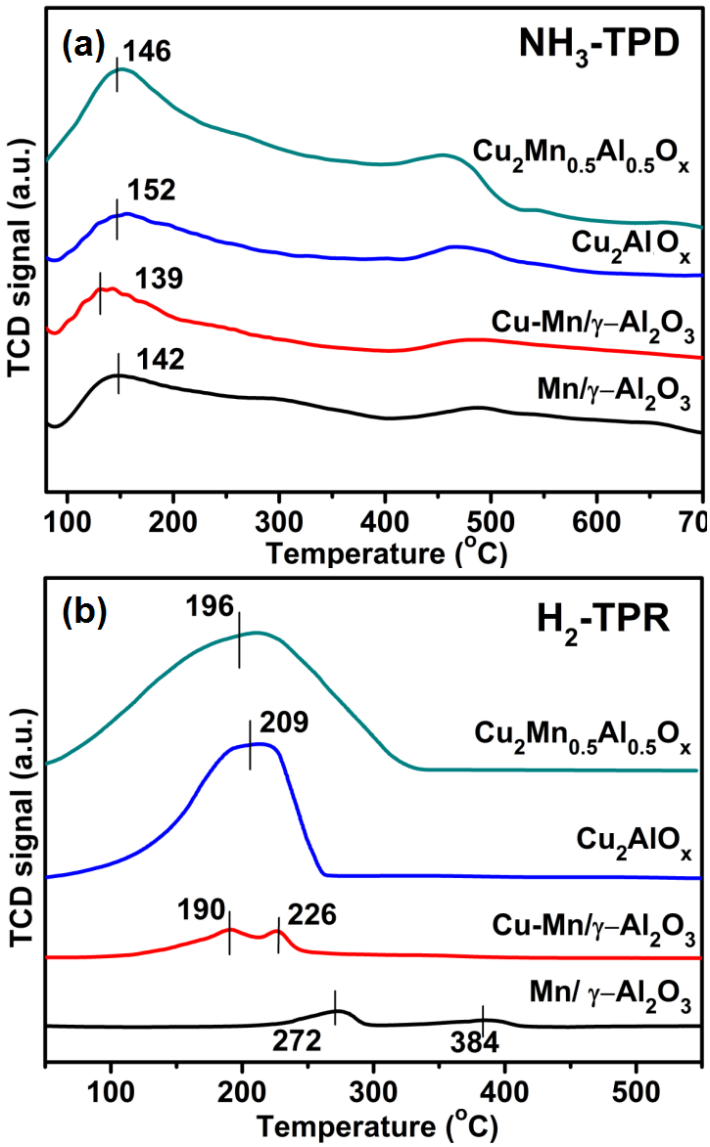

Fig. 7. (a) NH_3-TPD profiles over the $Cu_2Mn_{0.5}Al_{0.5}O_x$, Cu_2AlO_x, Cu-Mn/γ-Al_2O_3, and Mn/γ-Al_2O_3 catalysts, (b) H_2-TPR profiles over the $Cu_2Mn_{0.5}Al_{0.5}O_x$, Cu_2AlO_x, Cu-Mn/γ-Al_2O_3, and Mn/γ-Al_2O_3 catalysts.

3.4 SO_2 and H_2O poisoning of catalysts

In practical working conditions, the effluent gases always contain a small amount of SO_2 and water vapor, which is a challenge for NH_3-SCR catalysts, especially for Mn-

based catalysts.[20] At first, SO_2 could react with NH_3 to form $(NH_4)_2SO_3$ and NH_4HSO_4, which did not decompose below 200 °C and finally deposited on catalyst surface, causing pore plugging of catalysts. In addition, SO_2 may react with the active components, which cause inactivation for the NH_3-SCR reaction. Thus, the influence of SO_2 on catalytic performance must be considered for NH_3-SCR catalysts. Fig. 8(a) shows the effects of 100 ppm SO_2 on the SCR activities of all four catalysts at 150 °C. After a small and temporary increase of the NO_x conversion, the catalytic activity decreased with time. It indicated that the effect of SO_2 on the activity of catalysts at low temperature was inhibited for a short time, but eventually resulted in catalyst poisoning. The decreased activity may be caused by tightly absorbed SO_2, formed sulfates and other species on the surface occupying the active sites (such as MnO_x, CuO), which consequently decreased the SCR activity. With 100 ppm SO_2 was added to the system, the NO_x conversion for $Cu_2Mn_{0.5}Al_{0.5}O_x$, Cu_2AlO_x, Cu-Mn/γ-Al_2O_3, and Mn/γ-Al_2O_3 catalysts was 64.9%, 57.2%, 49.3% and 45.5% after 1 h, and then decreased to 49.5%, 43.1%, 34.6% and 20.2% after 3h at 150 °C, respectively. It can be concluded that the catalysts prepared from LDH precursors had relatively better SO_2 resistance. The SO_2 poisoning mechanism for $Cu_2Mn_{0.5}Al_{0.5}O_x$ catalyst was investigated using FT-IR analyses. Fig. 8(b) shows the FT-IR spectra of fresh and pre-sulfated $Cu_2Mn_{0.5}Al_{0.5}O_x$ catalyst. Two new peaks located at 1128 and 1051 cm^{-1} were observed with the pre-sulfated $Cu_2Mn_{0.5}Al_{0.5}O_x$, which could be assigned to the SO_4^{2-} species on acid sites. [51]

In order to investigate the effect of SO_2 on the redox properties of catalysts, the fresh and pre-sulfated catalysts were characterized by H_2-TPR. As shown in Fig. 8(c, d), compared with fresh catalysts, the reduction peaks of pre-sulfated catalysts moved to higher temperatures. It is well recognized that the reduction peak temperature is an indication of reducibility, and lower reduction temperature means stronger

reducibility.[51] In addition, the reduction peak area of all the catalysts decreased, which indicated that SO_2 had negative effect on the reducibility of catalysts. For Mn/γ-Al_2O_3 catalyst, the two low-temperature peaks located at 272 and 384 °C greatly moved to 301 and 406 °C. However, after adding Cu to Mn/γ-Al_2O_3 catalyst, the reduction peak temperatures of Cu-Mn/γ-Al_2O_3 only slightly increased, from 190 and 226 °C to 219 and 255 °C. These data demonstrated that the addition of Cu can promote the SO_2 resistance of Mn-based SCR catalyst. For the $Cu_2Mn_{0.5}Al_{0.5}O_x$ and Cu_2AlO_x catalysts obtained from LDHs precursors, the reduction peak temperatures were still very low even after SO_2 presulfation, which only slightly increased from 196 and 209 °C to 221 and 230 °C, respectively. Comparing to Cu_2AlO_x, the redox peak somehow stronger and the peak temperature was slightly lower for $Cu_2Mn_{0.5}Al_{0.5}O_x$. This might be the reason why $Cu_2Mn_{0.5}Al_{0.5}O_x$ catalyst has the best SO_2 resistance among all studied catalysts.

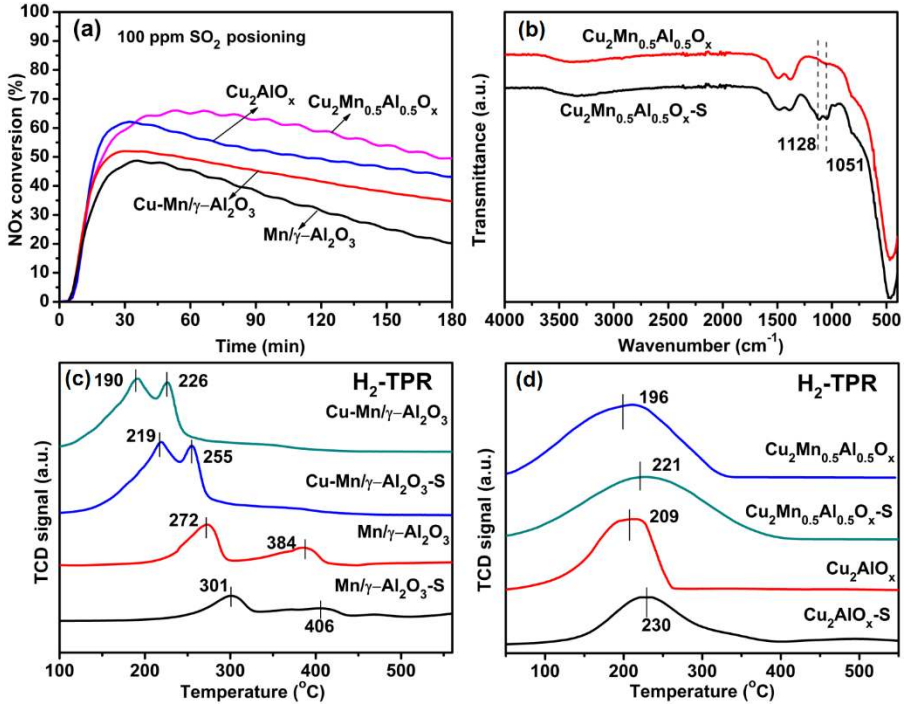

Fig. 8. (a) SCR activities of $Cu_2Mn_{0.5}Al_{0.5}O_x$, Cu_2AlO_x, Cu-Mn/γ-Al_2O_3, and Mn/γ-Al_2O_3 catalysts in the presence of SO_2, (b) FTIR spectra of $Cu_2Mn_{0.5}Al_{0.5}O_x$ and pre-

sulfated $Cu_2Mn_{0.5}Al_{0.5}O_x$, (c) H_2-TPR of fresh and pre-sulfated Cu-Mn/γ-Al_2O_3, and Mn/γ-Al_2O_3 catalysts, and (d) H_2-TPR of fresh and pre-sulfated $Cu_2Mn_{0.5}Al_{0.5}O_x$, and Cu_2AlO_x catalysts. Reaction conditions: [NO_x] = [NH_3] = 500 ppm, [O_2] = 5%, [SO_2] = 100 ppm, balance Ar, total flow rate = 200 mL/min, catalyst 0.15 g.

In addition, the SSA of fresh and deactivated catalysts are summarized in Table 3. The SSA for fresh $Cu_2Mn_{0.5}Al_{0.5}O_x$, Cu_2AlO_x, Cu-Mn/γ-Al_2O_3, and Mn/γ-Al_2O_3 was 136.4, 117.8, 144.6, and 135.6 m^2/g, respectively. After the sulfate species were formed and deposited on catalysts surface, the SSA of all sulfated $Cu_2Mn_{0.5}Al_{0.5}O_x$, Cu_2AlO_x, Cu-Mn/γ-Al_2O_3, and Mn/γ-Al_2O_3 became 127.4, 105.2, 103.9, and 100.4 m^2/g, respectively. It is apparent that the SSA of all samples decreased for a certain degree, which may be one reason that explains the decrease in catalytic activity. However, it is apparent that the SSA decreases for $Cu_2Mn_{0.5}Al_{0.5}O_x$ was much smaller than other catalysts, only 9 °C. In addition, the changes in pore size and pore volume of $Cu_2Mn_{0.5}Al_{0.5}O_x$ after SO_2 poisoning were also slight, which indicated that most of the sulfate species were deposited on the surface of catalysts, rather than in the micropores.[52] The BET analyses also confirmed that the $Cu_2Mn_{0.5}Al_{0.5}O_x$ catalyst is much more SO_2 resistant than the other controlled catalysts.

Table 3. Specific surface area, pore size, and pore volume of fresh and sulfated $Cu_2Mn_{0.5}Al_{0.5}O_x$, Cu_2AlO_x, Cu-Mn/γ-Al_2O_3, and Mn/γ-Al_2O_3.

Samples	BET SSA (m^2/g)	BJH Pore size (Å)	BJH pore volume (cm^3/g)
$Cu_2Mn_{0.5}Al_{0.5}O_x$	136.4	150.9	1.029414
Cu_2AlO_x	117.8	124.9	0.735527
Cu-Mn/γ-Al_2O_3	144.6	49.9	0.360984
Mn/γ-Al_2O_3	135.6	54.9	0.371907
$Cu_2Mn_{0.5}Al_{0.5}O_x$-S	127.4	150.1	0.955845
Cu_2AlO_x-S	105.2	66.3	0.874491

Cu-Mn/γ-Al_2O_3-S	103.9	63.1	0.674379
Mn/γ-Al_2O_3-S	100.4	61.2	0.613279

The effect of H_2O on the performance of catalysts was also tested. At 150 °C, the NO_x concentrations were recorded for 2 h, as shown in Fig. 9(a). In general, the existence of 5% H_2O showed visible NO_x conversion decreases at 150 °C for all catalysts. But $Cu_2Mn_{0.5}Al_{0.5}O_x$ was less influenced, with the NO_x conversion remained as high as 78.18%. Meanwhile, the NO_x conversions of Cu_2AlO_x, Cu-Mn/γ-Al_2O_3, and Mn/γ-Al_2O_3 catalysts were decreased to 63.64%, 46.02%, and 37.2% respectively. After stopping H_2O from the feed gases, the NO_x conversions can be restored to some extent, but still below the initial values, representing parts of the deactivation effect by H_2O is irreversible. The hindering effect by H_2O at low temperatures is mainly due to the competitive adsorption of H_2O with the reactants at the same active sites. Overall, this data suggests that $Cu_2Mn_{0.5}Al_{0.5}O_x$ catalyst also possesses much better H_2O resistance than the other catalysts studied in this work.

Fig. 9(b) compares the SCR activities of different catalysts in the presence of both SO_2 and H_2O simultaneously. After adding 5% H_2O and 100 ppm SO_2, the NO_x conversions of all catalysts decreased to certain degree within 2 h at 150 °C. Nevertheless, $Cu_2Mn_{0.5}Al_{0.5}O_x$ still showed the highest activity comparing to other three catalysts. The NO_x conversions of $CuMn_{0.5}Al_{0.5}O_x$, $Cu_2Mn_{0.5}Al_{0.5}O_x$, Cu_2AlO_x, Cu-Mn/γ-Al_2O_3, and Mn/γ-Al_2O_3 were about 62.18%, 49.6%, 41.5%, and 31.3% respectively. Upon removing H_2O and SO_2 from the feed gases, although the NO_x conversions could not return to their previous levels, they all were increased obviously. Particularly for $Cu_2Mn_{0.5}Al_{0.5}O_x$, the NO_x conversion was recovered from 62.18% to 80.7% after cutting down H_2O and SO_2.

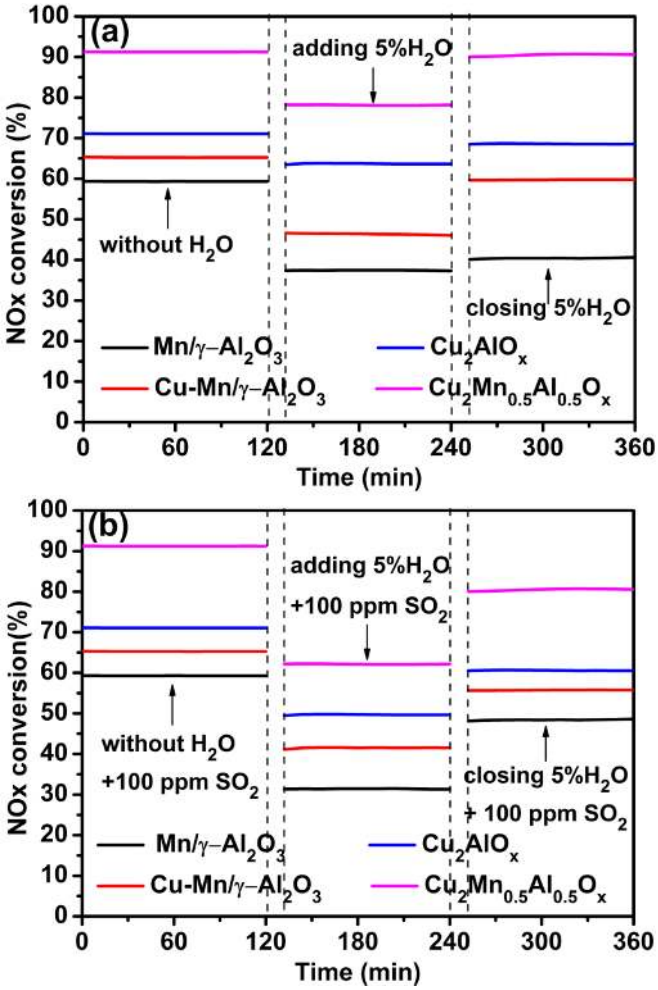

Fig. 9. (a) The effect of individual H_2O and (b) the effect of SO_2 and H_2O co-existence on the NO_x conversions over $Cu_2Mn_{0.5}Al_{0.5}O_x$, Cu_2AlO_x, Cu-Mn/γ-Al_2O_3 and Mn/γ-Al_2O_3 catalysts at 150 °C. Reaction conditions: [NO_x] = [NH_3] = 500 ppm, [O_2] = 5%, [H_2O] = 5%, [SO_2] = 100 ppm, balance Ar, total flow rate = 200 mL/min, catalyst 0.15 g.

3.5 Regeneration of deactivated catalysts

Considering the fact that the deactivation of catalysts can not be completely prevented, the regenerability of deactivated catalysts is also very important. In this study, thermal regeneration was selected to recover the catalytic activity of all deactivated catalysts. The deactivated catalyst was a vulcanized catalyst obtained after the above 100 ppm

SO_2 sulfur resistance test. Fig. 10(a) shows the NO_x conversion on the deactivated catalysts after thermal regeneration. The NO_x conversion on fresh $Cu_2Mn_{0.5}Al_{0.5}O_x$, Cu_2AlO_x, Cu-Mn/γ-Al_2O_3 and Mn/γ-Al_2O_3 were about 91.2%, 71.1%, 65.3% and 59.3% at 150 ℃, respectively. With 100 ppm SO_2 was added to the system, the NO_x conversion for $Cu_2Mn_{0.5}Al_{0.5}O_x$, Cu_2AlO_x, Cu-Mn/γ-Al_2O_3, and Mn/γ-Al_2O_3 catalysts was 34.2%, 28.3%, 22.4% and 8.1% after 12 h. After thermal regeneration, the catalytic activities of $Cu_2Mn_{0.5}Al_{0.5}O_x$, Cu_2AlO_x, Cu-Mn/γ-Al_2O_3 and Mn/γ-Al_2O_3 were recovered to 84.8%, 61.6%, 57.9, and 48.8%, respectively. In addition, the catalyst after the regeneration was also investigated using FT-IR analyses. Fig. 10(b) shows the FT-IR spectra of fresh, pre-sulfated, and regenerative $Cu_2Mn_{0.5}Al_{0.5}O_x$ catalyst. The peak belongs to SO_4^{2-} species apparently disappear after regeneration. It is indicated that most of sulfate and nitrate species deposited on the deactivated catalyst could be removed by thermal regeneration. These results clearly indicated that $Cu_2Mn_{0.5}Al_{0.5}O_x$ has much better regenerability and greater potential for practical applications than Cu_2AlO_x, Cu-Mn/γ-Al_2O_3, and Mn/γ-Al_2O_3 catalysts.

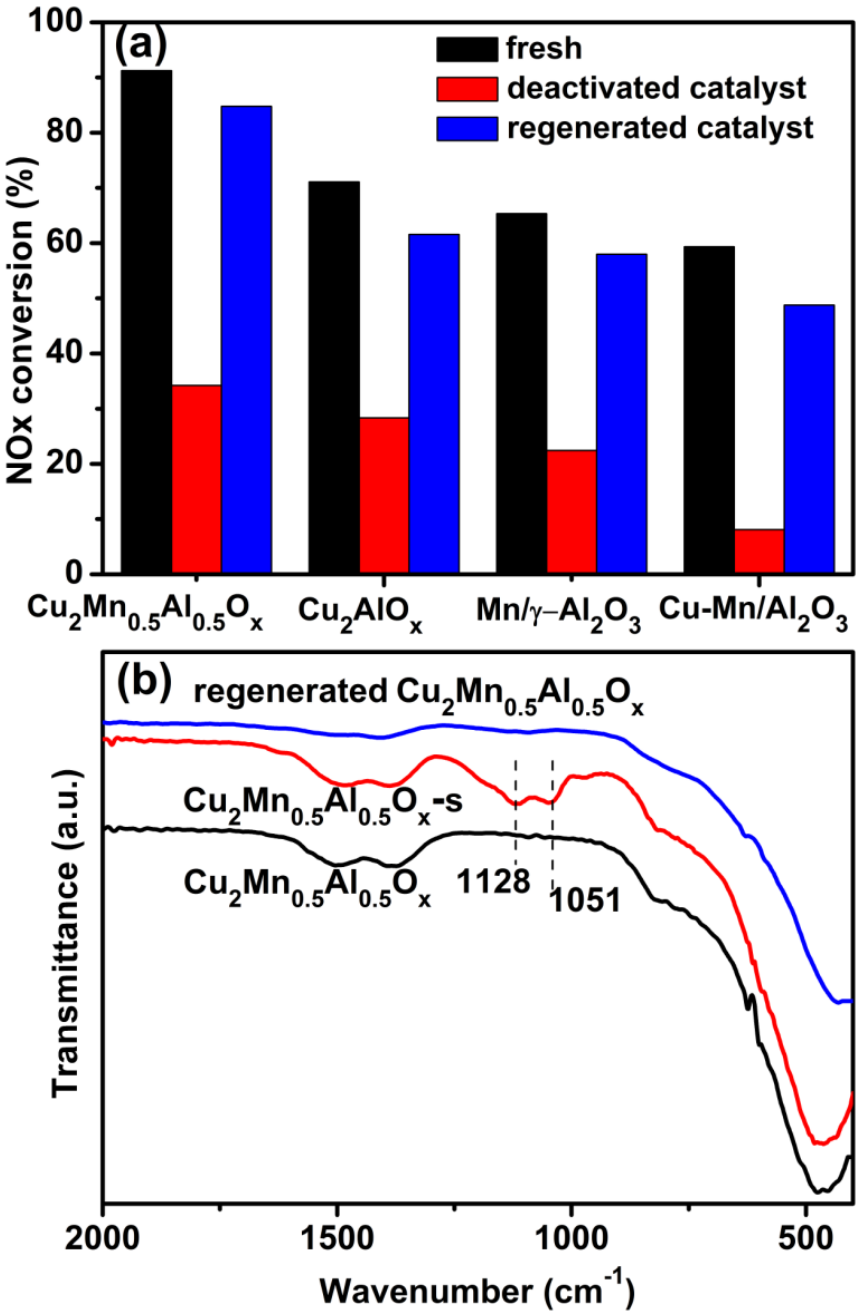

Fig. 10. (a) NO_x conversions of fresh, deactivated and regenerated catalysts treated by thermal regeneration, and (b) FTIR spectra of $Cu_2Mn_{0.5}Al_{0.5}O_x$, pre-sulfated $Cu_2Mn_{0.5}Al_{0.5}O_x$, and regenerated $Cu_2Mn_{0.5}Al_{0.5}O_x$, Reaction conditions: $[NO_x]$ = $[NH_3]$ = 500 ppm, $[O_2]$ = 5%, balance Ar, total flow rate = 200 mL/min, catalyst 0.15 g.

4. Conclusions

Highly dispersed $Cu_2Mn_{0.5}Al_{0.5}O_x$ mixed oxide was synthesized from the corresponding $Cu_2Mn_{0.5}Al_{0.5}$-CO_3 LDH as an excellent low-temperature NH_3-SCR catalyst. XRD, FTIR, SEM and TEM analyses demonstrated the successful synthesis of a series of "flower-like" LDHs, which are good precursors for the fabrication of highly dispersed $Cu_yMn_zAl_{1-z}O_x$ mixed oxide catalysts. The best catalyst $Cu_2Mn_{0.5}Al_{0.5}O_x$ showed much higher catalytic activity than the control catalyst Cu_2AlO_x, Cu-Mn/γ-Al_2O_3 and Mn/γ-Al_2O_3. The maximum NO_x conversions are 91.2%, 84.2%, 82.6%, and 67.2% for $Cu_2Mn_{0.5}Al_{0.5}O_x$, Cu_2AlO_x, Cu-Mn/γ-Al_2O_3 and Mn/γ-Al_2O_3, respectively. XRD and XPS analyses indicated that the $Cu_2Mn_{0.5}Al_{0.5}O_x$ catalyst mainly contains well dispersed MnO_2 and CuO nanoparticles, which are the main active components. In addition, the high concentrations of Mn^{4+} and Cu^{2+} should also be partly responsible for the good performance of $Cu_2Mn_{0.5}Al_{0.5}O_x$ catalyst. NH_3-TPD and H_2-TPR analyses indicated that $Cu_2Mn_{0.5}Al_{0.5}O_x$ possesses more acid sites and higher reducibility than other catalysts studied in this work. $Cu_2Mn_{0.5}Al_{0.5}O_x$ catalyst was also demonstrated to possess much better SO_2 and H_2O resistance than other control catalysts studied in this work. The regeneration studies of deactivated catalysts by thermal treatment at high temperatures indicated that the NO_x conversion of $Cu_2Mn_{0.5}Al_{0.5}O_x$ could be recovered to 84.8%, which is only slightly lower than its initial value (91.2%).

Acknowledgements

This work was supported by the Fundamental Research Funds for the Central Universities (2016ZCQ03), the National Natural Science Foundation of China (51622801, 51572029, and 51308045), and the Beijing Excellent Young Scholar (2015000026833ZK11).

References

1 W. Tian, H. Yang, X. Fan and X. Zhang, *J. Hazard. Mater.* , 2011, 188, 105-109.
2 S. Zhang, X. Liu, Q. Zhong and Y. Yao, *Catal. Commun.,* 2012, 25, 7-11.
3 G. A. Papapolymerou and L. D. Schmidt, *Langmuir,* 1985, 1, 488-495.
4 M. Kang, E. D. Park, J. M. Kim and J. E. Yie, *Appl. catal. A: general,* 2007, 327, 261-269.
5 J. R. Klovsky, P. B. Koradia and C. T. Lim, *Ind. Eng. Chem. Prod. Res. Dev.,* 1980, 19, 218-225.
6 H. Bosch and F. J. I. G. Janssen, *Catal. Today,* 1988, 2, 369-379.
7 G. Busca, L. Lietti, G. Ramis and F. Berti, *Appl. Catal. B: Environ.,* 1998, 18, 1-36.
8 W. S. Kijlstra, J. C. M. L. Daamen, J. M. van de Graaf, B. van der Linden, E. K. Poels and A. Bliek, *Appl. Catal. B: Environ.,* 1996, 7, 337-357.
9 J. Muniz, G. Marban and A. B. Fuertes, *Appl. Catal. B: Environ.,* 2000, 27, 27-36.
10 L. Singoredjo, R. Korver, F. Kapteijn and J. Moulijn, *Appl. Catal. B: Environ.,* 1992, 1, 297-316.
11 U. Bentrup, A. Brückner, M. Richter and R. Fricke, *Appl. Catal. B: Environ.,* 2001, 32, 229-241.
12 G. Qi, R. T. Yang and R. Chang, *Catal. Lett.,* 2003, 87, 67-71.
13 P. G. Smirniotis, D. A. Peña and B. S. Uphade, *Angew. Chem. Int. Ed.,* 2001, 40, 2479-2482.
14 G. Qi and R. T. Yang, *Appl. Catal. B: Environ.,* 2003, 44, 217-225.
15 M. Wallin, S. Forser, P. Thormählen and M. Skoglundh, *Ind. Eng. Chem. Res.,* 2004, 43, 7723-7731.
16 W. S. Kijlstra, D. S. Brands and E. K. Poels, *J. Catal.,* 1997, 171, 208-218.
17 B. Thirupathi and P. G. Smirniotis, *J. Catal.,* 2012, 288, 74-83.
18 Z. Wu, R. Jin, Y. Liu and H. Wang, *Catal. Commun.,* 2008, 9, 2217-2220.
19 B. Thirupathi and P. G. Smirniotis, *Appl. Catal. B: Environ.,* 2011, 110, 195-206.
20 M. Kang, E. D. Park, J. M. Kim and J. E. Yie, *Catal. Today,* 2006, 111, 236-241.
21 B. Jiang, Z. Li and S. C. Lee, *Chem. Eng. J.,* 2013, 225, 52-58.
22 M. Qiu, S. Zhan, H. Yu, D. Zhu and S. Wang, *Nanoscale,* 2015, 7, 2568-2577.
23 G. Xie, Z. Liu, Z. Zhu, Q. Liu, J. Ge and Z. Huang, *J. Catal.,* 2004, 224, 36-41.
24 G. Xie, Z. Liu, Z. Zhu, Q. Liu, J. Ge and Z. Huang, *J. Catal.,* 2004, 224, 42-49.
25 J. Wang, X. Mei, L. Huang, Q. Zheng, Y. Qiao, K. Zang, S. Mao, R. Yang, Z. Zhang, Y. Gao, Z. Guo, Z. Huang and Q. Wang, *J. Energy. Chem.,* 2015, 24, 127-137.
26 Q. Wang, H. H. Tay, D. J. W. Ng, L. Chen, Y. Liu, J. Chang, Z. Zhong, J. Luo and A. Borgna, *ChemSusChem,* 2010, 3, 965-973.
27 Q. Wang, Y. Gao, J. Luo, Z. Zhong, A. Borgna, Z. Guo and D. O'Hare, *RSC Advances,* 2013, 3, 3414-3420.

28 Q. Wang, H. H. Tay, L. Chen, Y. Liu, J. Chang, Z. Zhong, J. Luo and A. Borgna, *J. Nanoeng. Nanomanuf.,* 2011, 1, 298-303.
29 Y. Gao, Z. Zhang, J. Wu, X. Yi, A. Zheng, A. Umar, D. O'Hare and Q. Wang, *J. Mater. Chem. A,* 2013, 1, 12782-12790.
30 H. Yan, J. Lu, M. Wei, J. Ma, H. Li, J. He, D. G. Evans and X. Duan, *J. Mol. Struc.Theochem,* 2008, 866, 34-45.
31 F. Liu and H. He, *J. Phys. Chem. C,* 2010, 114, 16929-16936.
32 D. Yuan, X. Li, Q. Zhao, J. Zhao, M. Tadé and S. Liu, *J. Catal.,* 2014, 309, 268-279.
33 C. Gennequin, T. Barakat, H. L. Tidahy, R. Cousin, J. F. Lamonier, A. Aboukaïs and S. Siffert, *Catal. Today,* 2010, 157, 191-197.
34 B. Jiang, Y. Liu and Z. Wu, *J. Hazard. Mater.,* 2009, 162, 1249-1254.
35 M. Yu, C. Li, G. Zeng, Y. Zhou and X. Zhang, *Appl. Surf. Sci.,* 2015, 342, 174-182.
36 W. S. Kijlstra, M. Biervliet, E. K. Poels and A. Bliek, *Appl. Catal. B: Environ.,* 1998, 16, 327-337.
37 R. Mrad, R. Cousin, C. Poupin, A. Aboukaïs and S. Siffert, *Catal. Today,* 2015, 257, 98-103.
38 Z. Wu, B. Jiang and Y. Liu, *Appl. Catal. B: Environ.,* 2008, 79, 347-355.
39 K. Yamazaki, T. Suzuki, N. Takahashi, K. Yokota and M. Sugiura, *Appl. Catal. B: Environ.,* 2001, 30, 459-468.
40 A. S. Reddy, C. S. Gopinath and S. Chilukuri, *J. Catal.,* 2006, 243, 278-291.
41 F. Kapteijn, A. D. Vanlangeveld, J. A. Moulijn, A. Andreini, M. A. Vuurman, A. M. Turek, J.-M. Jehng and I. E. Wachs, *J. Catal.,* 1994, 150, 94-104.
42 X. Tang, J. Li, L. Sun and J. Hao, *Appl. Catal. B: Environ.,* 2010, 99, 156-162.
43 Y. Wu, Y. Lu, C. Song, Z. Ma, S. Xing and Y. Gao, *Catal. Today,* 2013, 201, 32-39.
44 C. Fang, D. Zhang, S. Cai, L. Zhang, L. Huang, H. Li, P. Maitarad, L. Shi, R. Gao and J. Zhang, *Nanoscale,* 2013, 5, 9199-9207.
45 L. Chen, J. Li and M. Ge, *Chem. Eng. J.,* 2011, 170, 531-537.
46 Q. Li, H. Yang, F. Qiu and X. Zhang, *J. hazard. mater.,* 2011, 192, 915-921.
47 F. Liu, H. He, C. Zhang, Z. Feng, L. Zheng, Y. Xie and T. Hu, *Appl. Catal. B: Environ.,* 2010, 96, 408-420.
48 J. Zhu, F. Gao, L. Dong, W. Yu, L. Qi, Z. Wang, L. Dong and Y. Chen, *Appl. Catal. B: Environ.,* 2010, 95, 144-152.
49 B. Liu, Y. Liu, C. Li, W. Hu, P. Jing, Q. Wang and J. Zhang, *Appl. Catal. B: Environ.,* 2012, 127, 47-58.
50 Y. Xiong, C. Tang, X. Yao, L. Zhang, L. Li, X. Wang, Y. Deng, F. Gao and L. Dong, *Appl. Catal. A: general,* 2015, 495, 206-216.
51 Q. Yan, Y. Nie, R. Yang, Y. Cui, H. O, D. and Q. Wang, *Appl. catal. A: general,* 2017, 538, 37-50.
52 Z. Sheng, Y. Hu, J. Xue, X. Wang and W. Liao, *J. Rare Earths,* 2012, 30, 676-682.